THE JOURNAL OF PHYSICAL CHEMISTRY Letters

Letter

Cite This: J. Phys. Chem. Lett. 2018, 9, 6232−6237

pubs.acs.org/JPCL

Controlled Molecular Assembly via Dynamic Confinement of Solvent

Jiali Zhang,[†] Victoria A. Piunova,[‡] Yang Liu,[†] Andy Tek,[‡] Qingbo Yang,[†] Jane Frommer,[‡] Gang-yu Liu,*[,†] and Joseph Sly[‡,§]

[†]Department of Chemistry, University of California, Davis, California 95616, United States

[‡]IBM Almaden Research Center, 650 Harry Road, San Jose, California 95120, United States

ABSTRACT: Assembly from ultrasmall solution droplets follows a different dynamic from that of larger scales. Using an independently controlled microfluidic probe in an atomic force microscope, subfemtoliter aqueous droplets containing polymers produce well-defined features with dimensions as small as tens of nanometers. The initial shape of the droplet and the concentration of solute within the droplet play significant roles in the final assembly of polymers due to the ultrafast evaporation rate and spatial confinement by the small droplets. These effects are used to control the final molecular assembly in terms of feature geometry and distribution and packing of individual molecules within the features. This work introduces new means of control over molecular assembly, bringing us closer to programmable synthesis for chemistry and materials science. The outcomes pave the way for three-dimensional (3D) nanoprinting in additive manufacturing.

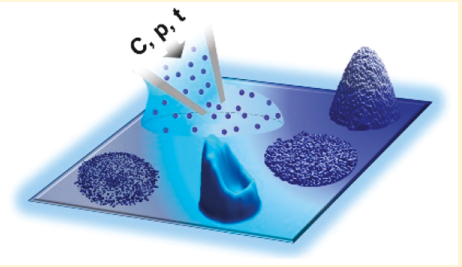

Assembly of molecules into mesoscale structures by design still poses great challenges, despite great advances in bottom-up and top-down approaches.[1,2] Self-assembly (SA) provides a good solution, such as self-assembled monolayers (SAMs),[3−5] phase-separated polymers,[6,7] and lipid bilayers.[8,9] Although powerful, SA is most effective in forming ordered structures or molecular assemblies driven by thermodynamics. Controlling mesoscale structures is difficult for structures formed off of the thermodynamic equilibrium, such as kinetically trapped structures.[10] New approaches are needed to attain "molecular assembly by design" with a high degree of control, enabling production of a wider range of structures, materials, and functions. This work reports a new approach to address this challenge, using evaporation-driven assembly from ultrasmall droplets to provide a foundation for three-dimensional (3D) printing in additive manufacturing and its applications.[11−14]

Studies on solid residues upon evaporation of micro- to macrodroplets that contained simple particles (e.g., polystyrene or silica) provided important groundwork for our approach.[15−18] Various patterns formed that fell into the off-equilibrium molecular assembly category.[15−17] Two well-known extremes are referred to as the "coffee ring effect"[19,20] and "Marangoni flow."[21−23] The former is due to a faster evaporation rate at the edge of the droplet causing "center-to-edge" capillary flow to compensate for evaporation. Various ring- or branch-like structures formed due to the directionality of the outward flow of solutes during drying, followed by their pinning at the triple interfacial lines.[19−23] As a countermeasure to avoid the coffee-ring effect, surface tension gradients have been created between the edge and top of the droplet, leading to an inward flow.[22] For example, by using a temperature gradient from the top of the droplet to the contact surface and avoiding particle pinning, the vortex movement in fluid dynamics during drying results in a pile up of solutes at the center. This is known as the Marangoni or Gibbs−Marangoni effect.[21,23] Upon miniaturization of a liquid droplet, the questions arose as to whether the molecular assemblies would follow or deviate from either of the effects and how to utilize the outcome for molecular assembly.

Delivery of an ultrasmall droplet was achieved with an independent microfluidic probe on an atomic force microscopy (AFM) stage.[24−28] The probe−surface contact is illustrated in Figure 1 with the geometric parameters clearly indicated. The opening at the tip apex is 300 nm, behind which the delivery pressure ranges from −800 to 1000 mbar. By varying both the contact time and surface functionality, this configuration delivers aqueous droplets as small as 0.4 attoliter (aL), which is an order of magnitude smaller than that previously recorded.[29,30] To test solute assembly upon delivery of a small liquid droplet, we selected solute molecules with insignificant to repulsive intermolecular interactions in the solution so that assembly was primarily solvent-driven. Star polymers meet the criteria, with a nanogel core and amphiphilic arms emanating from the cross-linked hydrophobic core.[31−34] The structure of a representative star polymer, star $[(\text{polystyrene})_{34}\text{-}(\text{poly}(N,N\text{-dimethylaminoethyl methacrylate})_{40}]_{39}$, abbreviated as star $[PS_{34}PDMAEA_{40}]_{39}$, is depicted in Figure 1B.[33] In aqueous solution and at pH 6.5 (ambient), the arms of the star polymer are positively charged due to protonation of amine residues,[35,36] hence assuming an extended conformation. When forcing two polymer molecules closer, the net electrostatic interaction is repulsive and the overall entropy decreases, and it becomes thermodynamically

Received: August 8, 2018
Accepted: October 15, 2018
Published: October 15, 2018

DOI: 10.1021/acs.jpclett.8b02442
J. Phys. Chem. Lett. 2018, 9, 6232−6237

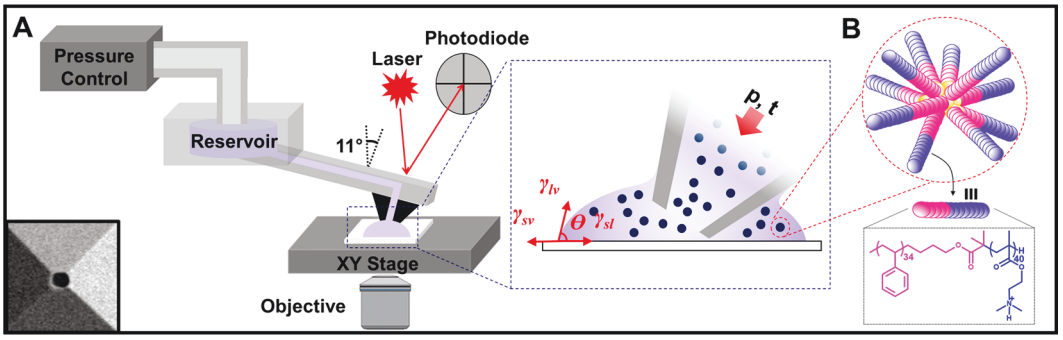

Figure 1. (A) Schematic diagram of an AFM with microfluidic delivery probe. An enlarged view of the probe–surface contact, illustrating the parameters of delivery (p, t), contact angle (θ), and surface tensions at phase boundaries (γ). The main axis of the square-pyramidal tip tilts 11° from the surface normal. The inset at the lower left is a SEM image of the nanopipette apex with a 300 nm aperture. (B) Schematic and chemical structure of star $[PS_{34}PDMAEMA_{40}]_{39}$.

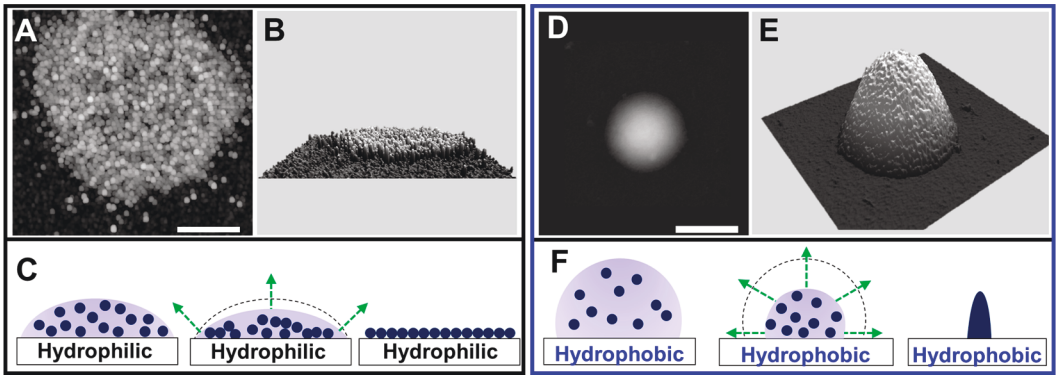

Figure 2. (A) AFM topographic image (1.8 μm × 1.8 μm) of a disk of star polymers formed on a hydrophilic AAPTMS/glass surface. (B) 3D display of image (A) where the feature height measures 5.5 ± 1.5 nm. (C) Schematic diagram illustrating the assembly of star polymers under constant contact area evaporation. (D) AFM topographic image (1.8 μm × 1.8 μm) of a mound of star polymers on a hydrophobic OTS/glass surface. (E) 3D display of image of (D) where the mound measures 90.4 nm tall. (F) Schematic diagram illustrating star polymer assembly under constant contact angle evaporation. Broken arrows (green) represent the evaporation direction and rate, and dashed lines (black) represent initial liquid–air boundaries. Scale bars = 500 nm.

unfavorable,[33,37] known as entropic repulsion (or electrostatic repulsion), thus preventing polymers from aggregating.[37−39] In fact, the star $[PS_{34}PDMAEMA_{40}]_{39}$ remained stable in aqueous solution for months under concentrations ranging from 2 × 10^{-6} to 3 × 10^{-5} M.

The shape of the droplet is determined by the surface hydrophilicity. Figure 2 compares the outcomes of star polymer assembly on hydrophilic vs hydrophobic surfaces upon delivery of droplets of subfemtoliter (fL) volume. The aqueous solution was made by mixing ethanol:glycerol:H_2O = 5:10:85 (v:v:v) and star $[PS_{34}PDMAEMA_{40}]_{39}$ into 1.305 × 10^{-5} M. The hydrophilic surfaces used were glass surfaces modified by *N*-(6-aminohexyl)-aminopropyltrimethoxysilane (AAPTMS) self-assembled monolayers. The solution contact angles on this SAM measured 53° and were thus hydrophilic or "solution-philic". Upon delivery of 170 aL of solution (p = 50 mbar, t = 1.08 s, and a contact force of 75 nN) and allowing ambient evaporation, the star polymers assembled into a disk 1.58 ± 0.15 μm in diameter and 5.5 ± 1.5 nm in height (Figure 2A,B). The height is similar to that of a monolayer of closely packed star polymers (4–6 nm) formed via polyelectrolyte (PE) coating protocols.[31] The molecules within the disk exhibit homogeneous distribution, with individual molecules clearly visible in an AFM topography image. The star–star nearest-neighbor (NN) separation is measured at around 39 ± 5 nm (Figure 2A), similar to that observed in the monolayer. This outcome of star polymer assembly is consistent with "constant contact area evaporation", whereupon delivery, sub-fL liquid quickly spread and evaporated on the solution-philic surface, covering a constant contact area (D = 1.58 μm), as shown in Figure 2C.[40−42] At 1.305 × 10^{-5} M concentration, (1.38 ± 0.12) × 10^3 star polymers assembled into a monolayer within the circle with NN separation of 39 nm. The result shown in Figure 2A has been repeated 36 times (6 × 6 arrays), and both robustness and versatility have been demonstrated by forming disks with diameters ranging from 0.7 to 7.1 μm by varying delivery t and p. These observations demonstrate molecular-level control over the outcome of the star polymer assembly, e.g., disk diameter and molecular packing within a disk, by predesigned initial conditions, such as p, t, contact angle, and solution concentration.

On hydrophobic substrates, such as glass surfaces derivatized with octadecyltrichlorosilane (OTS) SAMs, the same star polymer solution exhibited a contact angle of 97°, which is considered solution-phobic. Upon delivery of 90 aL of the solution and allowing evaporation under ambient conditions, the star polymers assembled into a mound 90.4 ± 1.5 nm tall and 0.636 ± 0.008 μm in diameter at the base (Figure 2D,E). This height is equivalent to 15 star polymer layers from PE desposition.[31] Though the substructure is clearly seen on the outer surface of the mound, individual star polymers are not recognizable in Figure 2E. The assembly into a mound shape is

DOI: 10.1021/acs.jpclett.8b02442
J. Phys. Chem. Lett. 2018, 9, 6232−6237

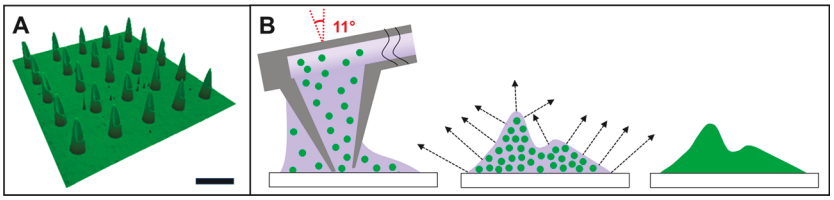

Figure 3. (A) 3D display of an AFM topograph (60 μm × 60 μm) showing the 5 × 5 arrays of symmetric star polymer assemblies. Scale bar = 10 μm. (B) Schematic diagram illustrating the characteristic moment of controlled assembly: during dispensing, immediately after probe withdrawal, and final assembly after solvent evaporation. Broken arrows indicate the evaporation direction and rate.

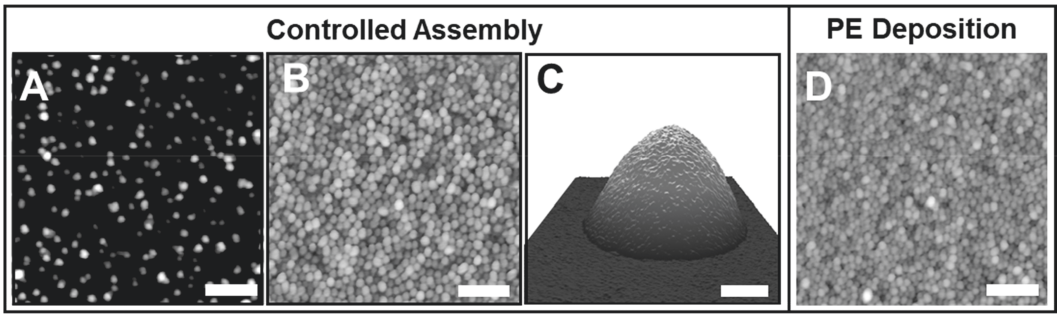

Figure 4. (A) AFM topographic image of star polymers assembled after dispensing 0.81 fL of 2.61 × 10^{-6} M solution on an AAPTMS/glass. (B) AFM topograph of a monolayer disk of closely packed star $[PS_{34}PDMAEMA_{40}]_{39}$ molecules. (C) 3D display of an AFM topography of a mound of interdigitated star polymers on an OTS/glass under the same p, t, and concentration as (B). (E) AFM topographic image of a monolayer of star $[PS_{34}PDMAEMA_{40}]_{39}$ on a glass surface following conventional PE deposition. Scale bars = 200 nm.

rationalized by the process of constant contact angle evaporation,[40,43,44] as illustrated in Figure 2F. The initial droplet beaded up on the OTS surface to a shape reminiscent of a spherical cap, in contrast to the spreading on AAPTMS SAMs. The ultrafast and near-constant-angle evaporation manifested as shrinkage of the droplet, until all solute molecules assembled into a smaller solid spherical cap. At a concentration of 1.305 × 10^{-5} M, the outcome is the mound observed in Figure 2E.

It may seem counterintuitive at first glance that positively charged star polymer molecules piled into a mound. From an energetic perspective, solvent evaporation into ambient increased the overall entropy of the system, thus overcoming the electrostatic repulsion among solute molecules. The power of the line tension is precedented in the context of maintaining the contact angle during evaporation to produce mound-like features at the micro- and millimeter scales.[45,46] In our case, as the droplet was smaller and evaporation occurred faster than microscopic deposition, the star polymer separation decreased rapidly under evaporation. The lack of independent individual star polymers in Figure 2E is consistent with interdigitation among polymer arms within the mound. Similar star polymers were known to collapse[47] and form gels under high concentration, e.g., amphiphilic heteroarm PE star polymers consisting of pure polystyrene and poly(2-vinylpyridine) arms.[48,49]

These observations have been reproduced 121 times (11 × 11 array of mounds). The robustness and versatility have been demonstrated by forming mounds ranging in height from 20 to 200 nm by varying delivery t and p. These suggest that one could attain a high degree of control over star polymer assembly by predesigned initial conditions such as p, t, contact angle, and concentration. From our time-dependent AFM imaging, all assembled structures exhibited high integrity and stability throughout the duration of our experiment, 5 months.

To further demonstrate the concept of "controlled assembly", geometries more complex than simple disks and mounds have been produced, again by well-designed initial conditions. Figure 3A shows 5 × 5 arrays of "cut-bamboo" or "bean bag" shaped features. Each feature was produced by dispensing 9.0 fL of star polymer solution onto a freshly cleaned glass surface. The delivery conditions were t = 0.5 s and p = 700 mbar with a contact force of 90 nN. The solution contained 2.61 × 10^{-5} M star $[PS_{34}PDMAEMA_{40}]_{39}$ in a mixed solvent of ethanol:H_2O = 1:9 (v:v). Clean glass surfaces were highly solution-philic (contact angle < 10°). Dynamic light scattering measured a star polymer diameter of 33.5 nm, i.e., stable without aggregation. This solvent exhibited a higher evaporation rate than that with previous experiments whose solvents contained a minute amount of glycerol. Each of the asymmetric features in Figure 3A had a base diameter of 3.61 ± 0.19 μm with an interior diameter of 1.10 ± 0.15 μm. The tall and short wedges were 88.9 ± 1.8 and 39.7 ± 2.1 nm in height, respectively, with 1.92 ± 0.11 μm separation. The saddle point measured 12.3 ± 1.7 nm above the surface. The formation of the asymmetric geometry is rationalized in Figure 3B. The probe is tilted 11° from the surface normal. As such, the liquid spread and accumulated around the silica exterior walls of the probe during delivery, forming an asymmetric droplet. Due to the high evaporation rate of the solvent, evaporation occurred immediately during delivery and upon withdrawal of the delivery probe. In contrast to the previous cases, where the liquid droplet relaxed to a spherical cap after dispensing (e.g., short and flat cap on hydrophilic surfaces and tall and narrow cap on hydrophobic surfaces), the fast evaporation worked against the surface tension and hindered the relaxation of this droplet. As a result, the star polymer assembled following approximately the initial geometry of the droplet wrapped around the tip, resulting in the asymmetric features. At high star polymer concentrations and ultrasmall droplets, the initial geometry dominated, thus the 1.92 μm

DOI: 10.1021/acs.jpclett.8b02442
J. Phys. Chem. Lett. 2018, 9, 6232−6237

separation as illustrated in Figure 3B. The results are reproducible as 37 bamboo features were produced consistently in two separate experiments. The robustness was also verified as the size and degree of asymmetry could be tuned by varying the volume of solutions, e.g., volcano shaped features were produced under shorter time and lower pressure. These observations demonstrate the impact of initial droplet geometry on the final feature geometry, which enables production of custom-designed geometry via programming initial droplet geometry, e.g., by custom-designed probes, or movement.

Control over the molecular packing within each feature was also achieved, as exemplified in Figure 4. Under the conditions of low concentration (e.g., 2.61×10^{-6} M star polymer in an EtOH:glycerol:H_2O = 1:10:89 solution) and a high degree of spreading (on AAPTMS/glass surfaces), 0.81 fL of droplet (p = 50 mbar, t = 1.33 s) yielded randomly distributed star polymers at submonolayer coverage (22.6%). The NN separation measured 90 ± 25 nm, twice as large as their hydrated diameter (47 nm), as shown in Figure 4A. To create closely packed structures with monolayer coverage, dense star polymers are required that cover the liquid−solid interface. Deposition of 1.78 fL of star polymer solution (1.305×10^{-5} M) under 200 mbar and 1.08 s onto AAPTMS/glass surfaces met the criteria, where the NN separation measured 37 ± 4 nm (Figure 4B). Bilayer and trilayer disks with closely packed star polymers could also be produced with increasing concentration. To force interdigitation among star polymers, solution-phobic surfaces were paired with a high concentration of solute (Figure 4C). In contrast, conventional PE deposition only resulted in a single-layer deposition, with a NN separation of 31 ± 5 nm (Figure 4D), similar to that of Figure 4B. In sum, our results demonstrate the feasibility of controlling molecular-level assembly within the feature.

Assembly of solute from ultrasmall droplets follows a different dynamic from that under larger scales. Using an independently controlled microfluidic probe in an atomic force microscope, this work reports our investigation into much reduced volumes, e.g., fL or smaller, using aqueous droplets containing positively charged star $[PS_{34}PDMAEMA_{40}]_{39}$. The results indicate that factors governing the assembly significantly differ from that of larger droplets as ultrasmall droplets exhibit ultrafast evaporation, and as such, the initial droplet geometry and concentration of the solute play dominant roles in dictating the final assembly of solute molecules. The feature geometry could be controlled by varying the initial droplet shapes to produce simple features such as disks and mounds and even asymmetric geometries. Control over the molecular packing within the features is also demonstrated ranging from a randomly distributed star polymer in a submonolayer to densely packed mono- and bilayer disks and interdigitated packing in mounds. Because controlling the initial droplet and solute distribution is much more achievable and programmable, this work represents a new paradigm to control the assembly of molecules. Work is in progress to analyze and model our systematic investigations to unveil the impacts of individual experimental parameters (t, p, T, surface functionality, and humidity) on the molecular assembly. Future work also includes monitoring and accurately measuring the evaporation process of ultrasmall droplets. The concepts and outcomes reported in this work pave the way for promising applications including 3D nanoprinting, programmable chemistry, and materials science.

EXPERIMENTAL METHODS

Materials. Glass slides (75 mm × 25 mm × 1 mm) were purchased from Fisher Scientific (Pittsburgh, PA). Glycerol (≥99%), sulfuric acid (H_2SO_4, 95.0−98.0%), hydrogen peroxide (H_2O_2, 30% aqueous solution), ammonium hydroxide (NH_4OH, 30% aqueous solution), tetrahydrofuran (THF, ≥99.9%), and toluene (99.8%) were purchased from Sigma-Aldrich (St. Louis, MO). *N*-(6-aminohexyl)-aminopropyltrimethoxysilane (AAPTMS) and octadecyltrichlorosilane (OTS) were purchased from Gelest (Morrisville, PA). Deuterated chloroform ($CDCl_3$) was purchased from Cambridge Isotopes (Tewksbury, MA). Ethanol (99.5%) was purchased from KPTEC (King of Prussia, PA). Milli-Q water (MQ water, 18.2 MΩ·cm at 25 °C) was produced by a Milli-Q water purification system (EMD Millipore, Billerica, MA). Nitrogen gas (99.999%) was purchased from Praxair, Inc. (Danbury, CT, King of Prussia, PA).

Synthesis and Characterization of Star Polymers. Star polymers used in this study were synthesized using a combined approach of anionic living polymerization and atom transfer radical polymerization (ATRP).[33] For $[PS_{34}PDMAEMA_{40}]_{39}$, indices 34 and 40 indicate the degree of polymerization of the arm, and 39 indicates the number of arms attached to the cross-linked polystyrene core. This star polymer is composed of a cross-linked polystyrene core and 39 independent arms of PS_{34}-*b*-$PDMAEMA_{40}$ diblock copolymer covalently linked to the core. The ^{1}H nuclear magnetic resonance (NMR) spectrum was captured using an Ascend 400 MHz (Bruker Instruments, Billerica, MA). Star $[PS_{34}PDMAEMA_{40}]_{39}$: ^{1}H NMR (400 MHz, $CDCl_3$, δ) = 7.13−6.49 (br s, 170H), 4.11 (br s, 80H), 2.63 (br s, 80H), 2.34 (br s, 240H), 1.84 (br s, 81H), 1.45 (br s, 34H), 1.08−0.92 (br m, 119H). The following abbreviations for multiplicity are used: s, singlet; m, multiplet; br, broad. It has a M_w: 383 kDa, polydispersity index (PDI) = 1.18, hydrodynamic radius (R_h in THF) = 13.8 nm, and glass transition temperature (T_g) = 45 °C, which were measured following the reported procedure.[33]

Zeta Potential and Hydrodynamic Size Measurement. A Zetasizer Nano ZS (Malvern Instruments, Malvern, U.K.) was used to measure the star polymer's zeta potential and hydrodynamic size.[31] Three solutions were first prepared: (1) stock solution was made by predissolving 100 mg of star $[PS_{34}PDMAEMA_{40}]_{39}$ powder in 1 mL of ethanol and then mixing it with 9 mL of MQ water to reach a final concentration of 2.61×10^{-5} M; (2) 100 μL of stock solution was mixed with 20 μL of glycerol and 80 μL of MQ water to reach a final concentration of 1.305×10^{-5} M; (3) 100 μL of stock solution was mixed with 100 μL glycerol and 800 μL of MQ water to reach a final concentration of 2.61×10^{-6} M. All solutions were then filtered through a 0.45 μm glass fiber filter prior to measurement. The refractive index, viscosity, and dielectric constant of the solvents were assumed to be the same as those of MQ water. Three measurements (10 runs each) were performed at 25 °C, and the average values were reported. The Smoluchowski approximation[50] was used to obtain the zeta potential of the particles. The zeta potential was measured to be 12.4, 15.3, and 19.6 mV for the above three solutions, respectively. The positive value of the zeta potential indicates the net positive charge of solute particles in solutions.

Preparation of Glass Supports. Glass slide substrates were first cleaned following established protocols.[51] Briefly, slides were soaked in piranha solution for 1 h, rinsed with a copious

DOI: 10.1021/acs.jpclett.8b02442
J. Phys. Chem. Lett. 2018, 9, 6232−6237

amount of MQ water. Piranha solution contains H_2SO_4 and H_2O_2 (v/v = 3:1), which should be handled with care for its high corrosiveness. The slides were then treated with a basic bath (mixture of NH_4OH, H_2O_2, and H_2O at a ratio of 5:1:1 (v/v)) for 1 h at 70 °C and then rinsed with a copious amount of MQ water followed by drying in nitrogen gas. Cleaned slides were modified using silane chemistry according to an established protocol.[52] Amine-terminated silane AAPTMS was prepared as follows: slides were heated at 70−80 °C in a sealed Teflon container (100 mL) containing 200 μL of AAPTMS for 2 h, then rinsed with ethanol and MQ water, and dried again in nitrogen gas. The OTS-modified glass slides were prepared by immersing slides in 5 mM OTS solution in toluene for 3 min, rinsing in toluene and ethanol, and drying in nitrogen gas. Contact angle data were then collected for the modified substrates with a VCA Optima Contact Angle Measurement system (AST Products, Billerica, MA) according to standard protocols.[53] A 3 μL drop of MQ water was placed on the substrate using a HPLC needle. At least three different positions per each sample were studied to confirm the surface wettability.

Integrated Microfluidic, AFM and Optical Microscope. A microfluidic system FluidFM Bot (Cytosurge, Glattbrugg, Switzerland)[24,25] was integrated with an AFM head, a precise $x-y$ stage, onto an inverted optical microscope (Olympus IX73, Olympus America, Center Valley, PA). The fluid-delivery cantilever probe (FluidFM Nanopipette, CYPR/001511, Cytosurge, Glattbrugg, Switzerland, 300 nm tip aperture at the apex of the square-pyramidal tip that tilts 11° from the surface normal; spring constant = 2 N/m) was made with a microchannel connected to a reservoir and controlled by a precise pressure controller. A digital camera (UI-3060CP-C-HQ, iDS Imaging Development Systems GmbH, Obersulm, Germany) was used for imaging. The pressure control was enabled by a mechanical pump and control system with a capacity range from −800 to +1000 mbar at a 1 mbar precision. Initially, 1 μL of the star polymer solution was filled into the probe's 2 μL reservoir using a Hamilton 7000 series syringe (Hamilton, Reno, NV).

AFM Imaging and Data Analysis. The star polymers and their constructs were characterized by AFM (MFP-3D, Oxford Instrument, Santa Barbara, CA). Silicon probes (AC 240-TS, Olympus America, Central Valley, PA) with a force constant of 1.7 N/m and resonant frequency of 70 kHz were used. Topography, amplitude, and phase images were acquired simultaneously using tapping mode. The driving frequency and damping were set at 70 kHz and 40%, respectively. Images were analyzed using Asylum MFP-3D software on an Igor Pro 6.12 platform. Particularly, the initial volume of droplets deposited on the hydrophilic surface was estimated from the total number of star polymers (N) (identified from a high-resolution AFM image using ImageJ (NIH)) and the solution concentration. For the droplet deposited on the hydrophobic surface, the volume was calculated based on the total star polymer number in the mound (total solid volume calculated based on the AFM measured height and diameter/individual star polymer volume) and the initial concentration in the solution.

AUTHOR INFORMATION

Corresponding Author

*E-mail: gyliu@ucdavis.edu. Tel: (530) 754-9678. Fax: (530) 754-8557.

ORCID

Jane Frommer: 0000-0002-5198-6127

Gang-yu Liu: 0000-0003-3689-0685

Notes

The authors declare no competing financial interest.

[§]J.S.: Author deceased.

ACKNOWLEDGMENTS

We wish to use this publication to honor our co-worker, Dr. Joseph Sly, a young and talented researcher at IBM Almaden Research Center, who untimely departed the world and our R&D effort. The authors gratefully acknowledge helpful discussions with Professor Roland Faller, Dr. Weifeng Lin, and Mr. Bradley Harris at UC Davis and Dr. Pablo Dörig at Cytosurge, Glattbrugg, Switzerland. Y.L. is supported in part by a UCD-LLNL Graduate Mentorship Award. This work is supported by the Gordon and Betty Moore Foundation and National Science Foundation (CHE-1808829).

REFERENCES

(1) Whitesides, G. M.; Grzybowski, B. Self-Assembly at All Scales. *Science* **2002**, *295*, 2418−2421.

(2) Xia, Y.; Whitesides, G. M. Soft Lithography. *Annu. Rev. Mater. Sci.* **1998**, *28*, 153−184.

(3) Bain, C. D.; Troughton, E. B.; Tao, Y. T.; Evall, J.; Whitesides, G. M.; Nuzzo, R. G. Formation of Monolayer Films by the Spontaneous Assembly of Organic Thiols from Solution onto Gold. *J. Am. Chem. Soc.* **1989**, *111*, 321−335.

(4) Sagiv, J. Organized Monolayers by Adsorption. 1. Formation and Structure of Oleophobic Mixed Monolayers on Solid Surfaces. *J. Am. Chem. Soc.* **1980**, *102*, 92−98.

(5) Nuzzo, R. G.; Allara, D. L. Adsorption of Bifunctional Organic Disulfides on Gold Surfaces. *J. Am. Chem. Soc.* **1983**, *105*, 4481−4483.

(6) De Rosa, C.; Park, C.; Thomas, E. L.; Lotz, B. Microdomain Patterns from Directional Eutectic Solidification and Epitaxy. *Nature* **2000**, *405*, 433−437.

(7) Hillmyer, M. A.; Bates, F. S.; Almdal, K.; Mortensen, K.; Ryan, A. J.; Fairclough, J. P. A. Complex Phase Behavior in Solvent-Free Nonionic Surfactants. *Science* **1996**, *271*, 976−978.

(8) Nagle, J. F.; Tristram-Nagle, S. Structure of Lipid Bilayers. *Biochim. Biophys. Acta, Rev. Biomembr.* **2000**, *1469*, 159−195.

(9) Groves, J. T.; Ulman, N.; Boxer, S. G. Micropatterning Fluid Lipid Bilayers on Solid Supports. *Science* **1997**, *275*, 651−653.

(10) Huang, J.; Xiao, Y.; Xu, T. Achieving 3-D Nanoparticle Assembly in Nanocomposite Thin Films Via Kinetic Control. *Macromolecules* **2017**, *50*, 2183−2188.

(11) Lewis, J. A. Direct Ink Writing of 3D Functional Materials. *Adv. Funct. Mater.* **2006**, *16*, 2193−2204.

(12) Therriault, D.; White, S. R.; Lewis, J. A. Chaotic Mixing in Three-Dimensional Microvascular Networks Fabricated by Direct-Write Assembly. *Nat. Mater.* **2003**, *2*, 265−271.

(13) Zhu, C.; Han, T. Y.-J.; Duoss, E. B.; Golobic, A. M.; Kuntz, J. D.; Spadaccini, C. M.; Worsley, M. A. Highly Compressible 3D Periodic Graphene Aerogel Microlattices. *Nat. Commun.* **2015**, *6*, 6962.

(14) Mueller, B. Additive Manufacturing Technologies−Rapid Prototyping to Direct Digital Manufacturing. *Assembly Automat* **2012**, DOI: 10.1108/aa.2012.03332baa.010.

(15) Singh, M.; Haverinen, H. M.; Dhagat, P.; Jabbour, G. E. Inkjet Printing—Process and Its Applications. *Adv. Mater.* **2010**, *22*, 673−685.

(16) Soltman, D.; Subramanian, V. Inkjet-Printed Line Morphologies and Temperature Control of the Coffee Ring Effect. *Langmuir* **2008**, *24*, 2224−2231.

DOI: 10.1021/acs.jpclett.8b02442
J. Phys. Chem. Lett. 2018, 9, 6232−6237

(17) Hu, H.; Larson, R. G. Analysis of the Effects of Marangoni Stresses on the Microflow in an Evaporating Sessile Droplet. *Langmuir* **2005**, *21*, 3972−3980.
(18) Malinowski, R.; Volpe, G.; Parkin, I. P.; Volpe, G. Dynamic Control of Particle Deposition in Evaporating Droplets by an External Point Source of Vapor. *J. Phys. Chem. Lett.* **2018**, *9*, 659−664.
(19) Han, W.; Lin, Z. Learning from "Coffee Rings": Ordered Structures Enabled by Controlled Evaporative Self-Assembly. *Angew. Chem., Int. Ed.* **2012**, *51*, 1534−1546.
(20) Deegan, R. D.; Bakajin, O.; Dupont, T. F.; Huber, G.; Nagel, S. R.; Witten, T. A. Capillary Flow as the Cause of Ring Stains from Dried Liquid Drops. *Nature* **1997**, *389*, 827−829.
(21) Scriven, L.; Sternling, C. The Marangoni Effects. *Nature* **1960**, *187*, 186−188.
(22) Hu, H.; Larson, R. G. Marangoni Effect Reverses Coffee-Ring Depositions. *J. Phys. Chem. B* **2006**, *110*, 7090−7094.
(23) Jeon, N. L.; Dertinger, S. K.; Chiu, D. T.; Choi, I. S.; Stroock, A. D.; Whitesides, G. M. Generation of Solution and Surface Gradients Using Microfluidic Systems. *Langmuir* **2000**, *16*, 8311−8316.
(24) Ventrici de Souza, J.; Liu, Y.; Wang, S.; Dörig, P.; Kuhl, T. L.; Frommer, J.; Liu, G.-y. Three-Dimensional Nanoprinting via Direct Delivery. *J. Phys. Chem. B* **2018**, *122*, 956−962.
(25) Deng, W. N.; Wang, S.; Ventrici de Souza, J.; Kuhl, T. L.; Liu, G.-y. New Algorithm to Enable Construction and Display of 3D Structures from Scanning Probe Microscopy Images Acquired Layer-by-Layer. *J. Phys. Chem. A* **2018**, *122*, 5756−5763.
(26) Kang, W.; McNaughton, R. L.; Yavari, F.; Minary-Jolandan, M.; Safi, A.; Espinosa, H. D. Microfluidic Parallel Patterning and Cellular Delivery of Molecules with a Nanofountain Probe. *J. Lab. Autom.* **2014**, *19*, 100−109.
(27) Gruter, R. R.; Voros, J.; Zambelli, T. FluidFM as a Lithography Tool in Liquid: Spatially Controlled Deposition of Fluorescent Nanoparticles. *Nanoscale* **2013**, *5*, 1097−1104.
(28) Fabié, L.; Agostini, P.; Stopel, M.; Blum, C.; Lassagne, B.; Subramaniam, V.; Ondarçuhu, T. Direct Patterning of Nanoparticles and Biomolecules by Liquid Nanodispensing. *Nanoscale* **2015**, *7*, 4497−4504.
(29) Meister, A.; Liley, M.; Brugger, J.; Pugin, R.; Heinzelmann, H. Nanodispenser for Attoliter Volume Deposition Using Atomic Force Microscopy Probes Modified by Focused-Ion-Beam Milling. *Appl. Phys. Lett.* **2004**, *85*, 6260−6262.
(30) Fabié, L.; Ondarçuhu, T. Writing with Liquid Using a Nanodispenser: Spreading Dynamics at the Sub-Micron Scale. *Soft Matter* **2012**, *8*, 4995−5001.
(31) Diep, J.; Tek, A.; Thompson, L.; Frommer, J.; Wang, R.; Piunova, V.; Sly, J.; La, Y.-H. Layer-by-Layer Assembled Core−Shell Star Block Copolymers for Fouling Resistant Water Purification Membranes. *Polymer* **2016**, *103*, 468−477.
(32) Appel, E. A.; Lee, V. Y.; Nguyen, T. T.; McNeil, M.; Nederberg, F.; Hedrick, J. L.; Swope, W. C.; Rice, J. E.; Miller, R. D.; Sly, J. Toward Biodegradable Nanogel Star Polymers via Organocatalytic Rop. *Chem. Commun.* **2012**, *48*, 6163−6165.
(33) Lee, V. Y.; Havenstrite, K.; Tjio, M.; McNeil, M.; Blau, H. M.; Miller, R. D.; Sly, J. Nanogel Star Polymer Architectures: A Nanoparticle Platform for Modular Programmable Macromolecular Self-Assembly, Intercellular Transport, and Dual-Mode Cargo Delivery. *Adv. Mater.* **2011**, *23*, 4509−4515.
(34) Ren, J. M.; McKenzie, T. G.; Fu, Q.; Wong, E. H. H.; Xu, J.; An, Z.; Shanmugam, S.; Davis, T. P.; Boyer, C.; Qiao, G. G. Star Polymers. *Chem. Rev.* **2016**, *116*, 6743−6836.
(35) Hage, W.; Liedl, K. R.; Hallbrucker, A.; Mayer, E. Carbonic Acid in the Gas Phase and Its Astrophysical Relevance. *Science* **1998**, *279*, 1332−1335.
(36) Vuoriluoto, M.; Orelma, H.; Johansson, L. S.; Zhu, B. L.; Poutanen, M.; Walther, A.; Laine, J.; Rojas, O. J. Effect of Molecular Architecture of PDMAEMA−POEGMA Random and Block Copolymers on Their Adsorption on Regenerated and Anionic Nanocelluloses and Evidence of Interfacial Water Expulsion. *J. Phys. Chem. B* **2015**, *119*, 15275−15286.
(37) Jusufi, A.; Likos, C.; Löwen, H. Counterion-Induced Entropic Interactions in Solutions of Strongly Stretched, Osmotic Polyelectrolyte Stars. *J. Chem. Phys.* **2002**, *116*, 11011−11027.
(38) Lowack, K.; Helm, C. Molecular Mechanisms Controlling the Self-Assembly Process of Polyelectrolyte Multilayers. *Macromolecules* **1998**, *31*, 823−833.
(39) Dobrynin, A. V.; Rubinstein, M. Theory of Polyelectrolytes in Solutions and at Surfaces. *Prog. Polym. Sci.* **2005**, *30*, 1049−1118.
(40) Chhasatia, V. H.; Sun, Y. Interaction of Bi-Dispersed Particles with Contact Line in an Evaporating Colloidal Drop. *Soft Matter* **2011**, *7*, 10135−10143.
(41) Ko, H.-Y.; Park, J.; Shin, H.; Moon, J. Rapid Self-Assembly of Monodisperse Colloidal Spheres in an Ink-Jet Printed Droplet. *Chem. Mater.* **2004**, *16*, 4212−4215.
(42) Park, J.; Moon, J. Control of Colloidal Particle Deposit Patterns within Picoliter Droplets Ejected by Ink-Jet Printing. *Langmuir* **2006**, *22*, 3506−3513.
(43) Erbil, H. Y.; McHale, G.; Newton, M. Drop Evaporation on Solid Surfaces: Constant Contact Angle Mode. *Langmuir* **2002**, *18*, 2636−2641.
(44) Kuncicky, D. M.; Velev, O. D. Surface-Guided Templating of Particle Assemblies inside Drying Sessile Droplets. *Langmuir* **2008**, *24*, 1371−1380.
(45) Ciszek, J. W.; Huang, L.; Tsonchev, S.; Wang, Y.; Shull, K. R.; Ratner, M. A.; Schatz, G. C.; Mirkin, C. A. Assembly of Nanorods into Designer Superstructures: The Role of Templating, Capillary Forces, Adhesion, and Polymer Hydration. *ACS Nano* **2010**, *4*, 259−266.
(46) Gibaud, T.; Barry, E.; Zakhary, M. J.; Henglin, M.; Ward, A.; Yang, Y.; Berciu, C.; Oldenbourg, R.; Hagan, M. F.; Nicastro, D.; et al. Reconfigurable Self-Assembly through Chiral Control of Interfacial Tension. *Nature* **2012**, *481*, 348−351.
(47) Uhlík, F.; Košovan, P.; Zhulina, E. B.; Borisov, O. V. Charge-Controlled Nano-Structuring in Partially Collapsed Star-Shaped Macromolecules. *Soft Matter* **2016**, *12*, 4846−4852.
(48) Shusharina, N. P.; Rubinstein, M. Concentration Regimes in Solutions of Polyelectrolyte Stars. *Macromolecules* **2008**, *41*, 203−217.
(49) Kyriazis, A.; Aubry, T.; Burchard, W.; Tsitsilianis, C. Colloidal Gel from Amphiphilic Heteroarm Polyelectrolyte Stars in Aqueous Media. *Polymer* **2009**, *50*, 3204−3210.
(50) Sze, A.; Erickson, D.; Ren, L.; Li, D. Zeta-Potential Measurement Using the Smoluchowski Equation and the Slope of the Current−Time Relationship in Electroosmotic Flow. *J. Colloid Interface Sci.* **2003**, *261*, 402−410.
(51) Liu, Y.; Wang, K.-H.; Chen, H.-Y.; Li, J.-R.; Laurence, T. A.; Ly, S.; Liu, F.-T.; Liu, G.-Y. Periodic Arrangement of Lipopolysaccharides Nanostructures Accelerates and Enhances the Maturation Processes of Dendritic Cells. *ACS Appl. Nano Mater.* **2018**, *1*, 839−850.
(52) Lin, W.-f.; Swartz, L. A.; Li, J.-R.; Liu, Y.; Liu, G.-y. Particle Lithography Enables Fabrication of Multicomponent Nanostructures. *J. Phys. Chem. C* **2013**, *117*, 23279−23285.
(53) Jung, M.-H.; Choi, H.-S. Characterization of Octadecyltrichlorosilane Self-Assembled Monolayers on Silicon (100) Surface. *Korean J. Chem. Eng.* **2009**, *26*, 1778−1784.

DOI: 10.1021/acs.jpclett.8b02442
J. Phys. Chem. Lett. 2018, 9, 6232−6237